Article

A Comparative Study to Evaluate the Essential Work of Fracture to Measure the Fracture Toughness of Quasi-Brittle Material

Mohammed Y. Abdellah [1,2,*], Abdul-Rahman Zuwawi [1], Sufyan A. Azam [1] and Mohamed K. Hassan [1,3]

1   Mechanical Engineering Department, College of Engineering and Islamic Architecture,
    Umm Al-Qura University, Makkah 21955, Saudi Arabia; s44280337@st.uqu.edu.sa (A.-R.Z.);
    saazam@uqu.edu.sa (S.A.A.); mkibrahiem@uqu.edu.sa (M.K.H.)
2   Mechanical Engineering Department, Faculty of Engineering, South Valley University, Qena 83523, Egypt
3   Production Engineering and Design Department, Faculty of Engineering, Minia University,
    Minia 61111, Egypt
*   Correspondence: myahmad@uqu.edu.sa

Abstract: In the present work, three different woven composite laminates were fabricated using the hand lay-up method. The woven reinforcement fibres were carbon fibres (CFRP), glass fibres (GFRP-W) and (GFRP-R) in combination with epoxy resin. Then, the central notch specimen tensile test (CNT) was used to measure the fracture toughness and the corresponding surface release energy (G_{IC}). Then, the data were compared with the essential work of fracture (we) values based on the stored energy of the body to obtain a new standard fracture toughness test for composite laminates using relatively simple techniques. In addition to an extended finite element model, XFEM was implemented over a central notch specimen geometry to obtain a satisfactory validation of the essential work of fracture concepts. Therefore, the average values of (G_{IC}) were measured with CNT specimens 25.15 kJ/m^2, 32.5 kJ/m^2 and 20.22 kJ/m^2 for CFRP, GFRP-W and GFRP-R, respectively. The data are very close as the percentage error for the surface release energy measured by the two methods was 0.83, 4.6 and 5.16 for carbon, glass and random fibre composite laminates, respectively. The data for the fracture toughness of XFEM are also very close. The percentage error is 4.6, 5.25 and 2.95 for carbon, glass and random fibre composite laminates, respectively. Therefore, the fundamental work of the fracture concept is highly recommended as a fracture toughness test for composite laminates or quasi-brittle Material.

Keywords: fracture; linear elastic; laminates; mode I; quasi-brittles

1. Introduction

Quasi-brittle material is characterised by an intermediate zone before the crack tip between fully linear material (brittle) and non-linear material (ductile) [1–3]. The fracture toughness of quasi-brittle materials, such as tough ceramics, ice and reinforced laminates, is of great importance for the description and characterisation of their applications [4]. These types of materials are particularly sought after in applications where specific gravity is an issue, such as aerospace [5], marine, offshore [6] and automotive [7]. Fracture toughness or crack resistance is one of the most important properties as it has a great influence on the damage and failure mechanisms of such composite structures. Linear elastic fracture mechanics has introduced many standard specimens with different shapes and geometries for fracture toughness testing, such as compact tension, centre notch tension, edge notch tension and single edge notch bending [8]. There is no standard for reinforced composite laminates. The compact tensile test has been commonly used for fracture toughness testing of unidirectional fibre composite laminates as reported in [9,10], while the central notch tensile specimen (CNT) test was introduced for multidirectional composite laminates by Soutis et al. [11] due to its simplicity and applicability.

The essential work of fracture (EWF) method uses a different criterion that does not depend on the LEFM and J-integral concepts, but on the strip length and the total work and energy stored in a cracked specimen [12]. In [13], the total work carried out by the action of the load in the fracture processing zone was divided into two parts: the essential work *(we)* corresponding to elastic deformation and the non-essential work *(wp)* corresponding to plastic deformation. For the LEFM concept, the EWF *(we)* is indicative of the crack propagation resistance or fracture toughness (G_{IC}) [14], but it is different from the value of the J-integral responsible for the concepts of elastic plastic fracture mechanics EPFM [15]. It should be recognised that the EWF *(we)* takes into account the crack initiation resistance (G_{IC}), if the variation in (G_{IC}) is small [14], then the relationship between the EWF *(we)* and the J-integral (J_i) is valid according to the EPFM [16]. On the other hand, EWF was characterised by its simplicity in data reduction, sample preparation and even evaluation, which made it attractive for measuring the fracture toughness of ductile thin films [17–19].

EWF was used early to measure the fracture toughness of thin plastic films, thin coatings and paints [20]. In addition, it was recommended by Martinez et al. [21] as a useful method for thin polymer materials. Recently, the EWF method was used by Pegoretti et al. [22] to measure the fracture toughness of low-density polyethylene films, reporting that the prepared notch affected the results of the linear regression coefficient of EWF and the non-essential work of fracture was lower than that of EWF. Moreover, the increase in specimen thickness led to a propagation of the constriction zone in front of the crack tip, so that the fracture toughness (J_C), the EWF and the crack opening motion were influenced by the thickness [23,24]. The ligament length was not chosen arbitrarily. When the fracture toughness was tested using the EWF method on low-density polyethylene, Zn and Al alloys, it was concluded that the exact choice of ligament length affected the generation of the linear regression [25]. In addition, other works [18,26,27] measured the fracture toughness with EWF to standardise it for polymeric materials with thin or relatively thick thickness. On the other hand, the loading rate influenced the EWF evaluation for polymeric materials as cited by CHING, Emma CY et al. [28]. Furthermore, the EWF approach was extended to polymeric materials reinforced with carbon nanotubes, as in Tehran et al. [29], where the nanomaterial had an effect on reducing the fracture toughness measured by EWF assessment. Similarly, an opposite effect on the essential work of fracture and non-essential work of fracture parameters was found when nanofillers were added to the low thickness polymer composite material [30,31]. In an experiment by Hassan et al. [32], the concept of EWF was used to model the fracture toughness of hybrid composite laminates used in micromechanical systems. This type of material, where a thin copper layer was attached to a substrate of glass fibre composite laminates, behaves with a large plastic zone, making EWF an acceptable method for sandwich composite structure.

A numerical model proposed by Abdellah [33] used two finite element models, one called the extended finite element method based on a meshless free and an enhancement function, and another based on the J-integral method to correlate the relationship between the mode I fracture toughness (J_{IC}) and the EWF of ductile thin aluminium plates. Cohesive zone models, where a fictitious crack was introduced through the model, were used early in combination with FEMs, such as the cohesive element [34–37] and cohesive surface [36,38,39]. They were characterised by their robustness and good accuracy, but required more computational time. In addition, recently there was a novel and strong mesh-free technique that can be used for stress/rupture analysis (e.g., measurement of fracture toughness) of anisotropic media. This is the element-free Galerkin method for three-dimensional propagation based on a phase field model, which was proposed by Y. Shao et al. [40]. There was also a new technique, the Bezier-based multistep method, which was first derived for a 1D stress intensity factor problem based on the solution of the fourth-order differential equations of LEFM. This model was extended to 2D problems by Kabir, H., and Aghdam, M. M. [41].

As explained earlier, EWF is commonly used to measure the fracture toughness of very ductile, thin polymers with a fully failing softening zone. Therefore, it was extended to involve the composite-reinforced laminates.

The main idea of the present study is to obtain a simple standard method for measuring the fracture toughness of composite laminates with a mean plastic zone in front of the crack tips. To evaluate this main idea, the following objectives should be established: (1) measure the fracture toughness of carbon, glass and random fibre composite laminates using conventional standard specimens with a central notch, (2) develop an essential work of fracture (EWF) evaluation procedure to obtain alternative fracture toughness values, (3) creation of an extended finite element model (XFEM) to predict the fracture toughness of the reinforced/epoxy composite laminates using a standard tensile specimen with a central notch and (4) final comparison of the two methods to determine the applicability of the EWF aspects for measuring the fracture toughness of quasi-brittle materials such as composite laminates.

The methodology of the article is structured as follows: In the first section, the fundamentals of EWF are described and outlined. In the second section, the experimental matrix is presented and the fabrication techniques are explained. Furthermore, in the third section, the XFEM was derived and implemented using a linear elastic model for centre notch tension specimen. In the fourth section, the results of the fracture toughness tests are presented, discussed and compared. Finally, a conclusion is given with suggestions for the future study.

2. Analytical Model (Essential Work of Fracture)

The EWF method should be defined to understand the current model derivation that links EWF *(we)* to the critical J-integral (J_{IC}). New concepts are used to describe new assumptions. The EWF system is based on the work of Mai and Cotterell [42] and the recommendation of Broberg [43]. They proposed to divide the total energy consumed in ductile cracking into the work related to the formation of a developed fracture surface (referred to as "essential" work) and the work related to plastic deformation (referred to as "non-essential" work, which depends on the geometry of the plastic deformation). Figure 1 illustrates the procedure for determining the work required by creating a fracture surface in ordinary DENT specimens. The specimen is loaded in tension until the strip *L* yields completely at the maximum load and the two plastic zones that form at the crack tips come into contact [44]. Ductile cracks progress through the ligament until complete failure occurs. Figure 2a shows the curve of load versus displacement δ. As shown in Equations (1) and (2) [13,43,45,46], the total work of fracture (W_f) is defined as the sum of (W_e), the essential term, and (W_p), the non-essential term:

$$W_f = \int_0^\delta p \, d\delta \tag{1}$$

$$W_f = W_e + W_p \tag{2}$$

where (W_e) refers to the crack tip's instability and offers surface release work in the crack process zone and (W_p) refers to the plastic deformation zone behind the fracture process zone. In addition, δ is the failure displacement.
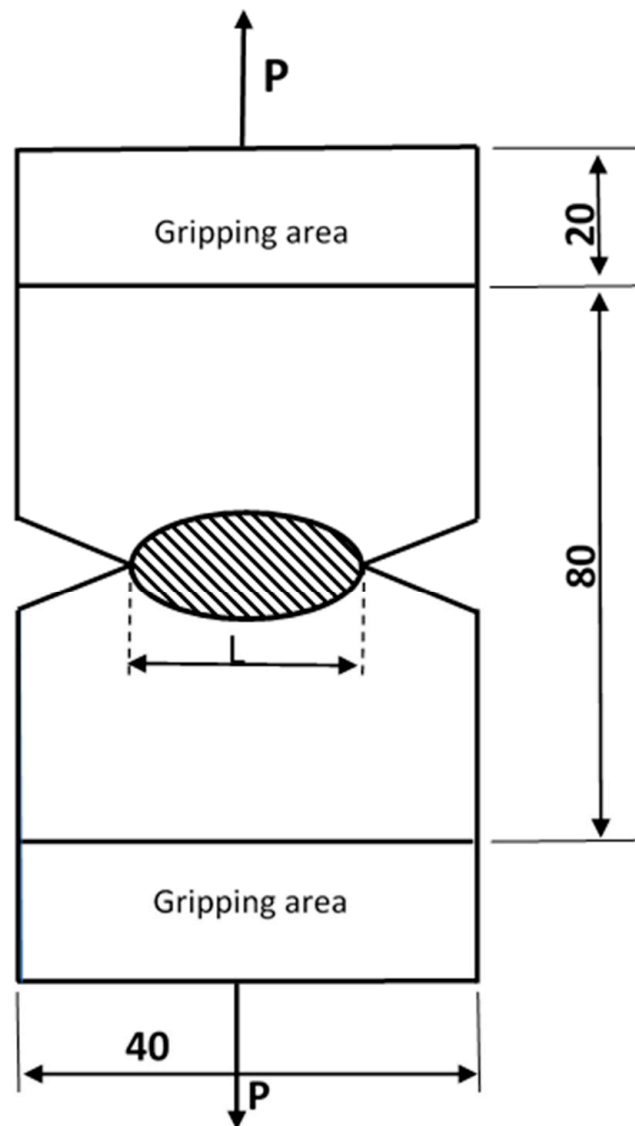
Figure 1. Double edge notch tension (DENT).
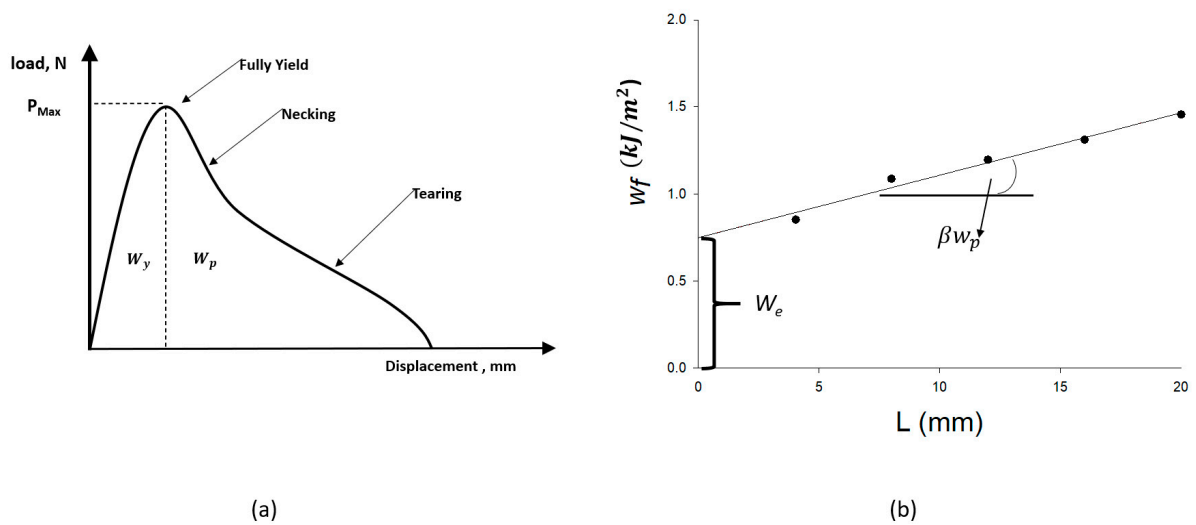
Figure 2. Essential work of fracture (**a**) load–displacement curve and (**b**) EWF fitting.

For a given specimen thickness, the surface work of liberation (W_e) is proportional to the length of the ligament L. (w_p) denotes the volume energy proportional to the volume (L^2t). To obtain an equation for the energy, divide Equation (2) by the ligament area (Lt) as follows:

$$w_f = \frac{W_f}{Lt} = w_e + \beta w_p L \tag{3}$$

where β is the shape factor of the plastic deformation and (w_p) is the specific non-essential work of the fracture and is considered as the plastic work per unit volume of the plastic deformation zone before the crack tip. In addition, we are the release energy of the surface required to initiate the formation of the fracture surface. The relationship of (w_f) given in Equation (3) is a linear regression related to the ligament length L. The positive intercept at $L = 0$ is the specific EWF, (w_e). The slope of the regression line is determined by fitting the data linearly with the non-essential work of fracture (w_p) (see Figure 2b).

For a DENT specimen, Equation (2) can be rewritten as follows after the application of a load and complete yielding of the strip:

$$W_f = W_y + W_{pp} \tag{4}$$

where (W_y) is the elastic zone's mechanical energy and (W_{pp}) is the plastic zone's plastic energy consumed for necking and subsequent tearing, as shown in Figure 2a.

(w_e) may divide the elastic zone of EWF; (w_y) associated with crack initiation and the plastic zone of EWF; and (w_{pp}) associated with ripping before necking ahead of the crack tip using Equation (4) as follows:

$$w_e = w_y + w_{pp} \tag{5}$$

In addition, the slope can be divided as follows:

$$\beta w_p = \beta y w_{py} + \beta p w_{pp} \tag{6}$$

where βy and βp are the geometric shape factors related to the plastic zone during ligament yielding and tearing after necking, respectively.

3. Methods and Material

3.1. Material and Manufacturing

Three different types of woven fibres are used as reinforcing material: carbon fibres, glass fibres and random fibres, while the matrix material is epoxy resin. The properties of these components are listed in Table 1 [47,48]. The composite laminate was constructed using the hand lay-up technique, which is the cheapest and most economical method [49,50]. The hand lay-up technique can be summarised as follows: (1) Two glass plates are used, with one plate serving as a base and coated with wax as a release agent to prevent sticking. (2) First a layer of epoxy is applied, followed by a layer of woven fibres, again a layer of epoxy is spread evenly with a brush and an aluminium roller is used to remove voids. (3) Repeat the previous step with the clean fibre layers until eight layers and the laminate are built up (Figure 3). (4) The second glass plate with release agent is placed over the entire layer. (5) Finally, a series of weights is placed over the second plate to obtain a relatively uniform thickness. The glass plate was removed after 24 h and the laminates were fully cured at room temperature for 21 days [51]. This system of curing offers ease of processing, high reliability and does not require thermal energy [52]. The mixing ratio was as recommended by the manufacturers, i.e., resin: hardener = 2:1 by weight. The fibre volume fraction was measured using the ignition technique according to the ASTM D3171-99 standard [53]. The mean values of volume fraction were found to be 65% for carbon-fibre-reinforced polymer (CFRP), 45% for glass-fibre-reinforced polymer (GFRP) and random-glass-fibre-reinforced polymer (RGFRP). The symbols S1, S2 and S3 refer to

CFRP, GFRP and RGFRP, respectively. The mean thickness (t) was 2.5 mm, 5 mm and 4 mm for S1, S2 and S3 materials, respectively.

Table 1. Mechanical and physical properties of E-glass fibre and epoxy resin [54–56].

Properties	E-Glass	AS4-Carbon Fibre	Kemapoxy (150RGL)
Density (kg/m^3)	2600	1790	1.2
Tensile strength (MPa)	3450	4270	85
Tensile modulus (GPa)	80	228	2.5
Passion ratio	0.25	0.34	0.35
In plane shear modulus (GPa)	30.8	25	1.24
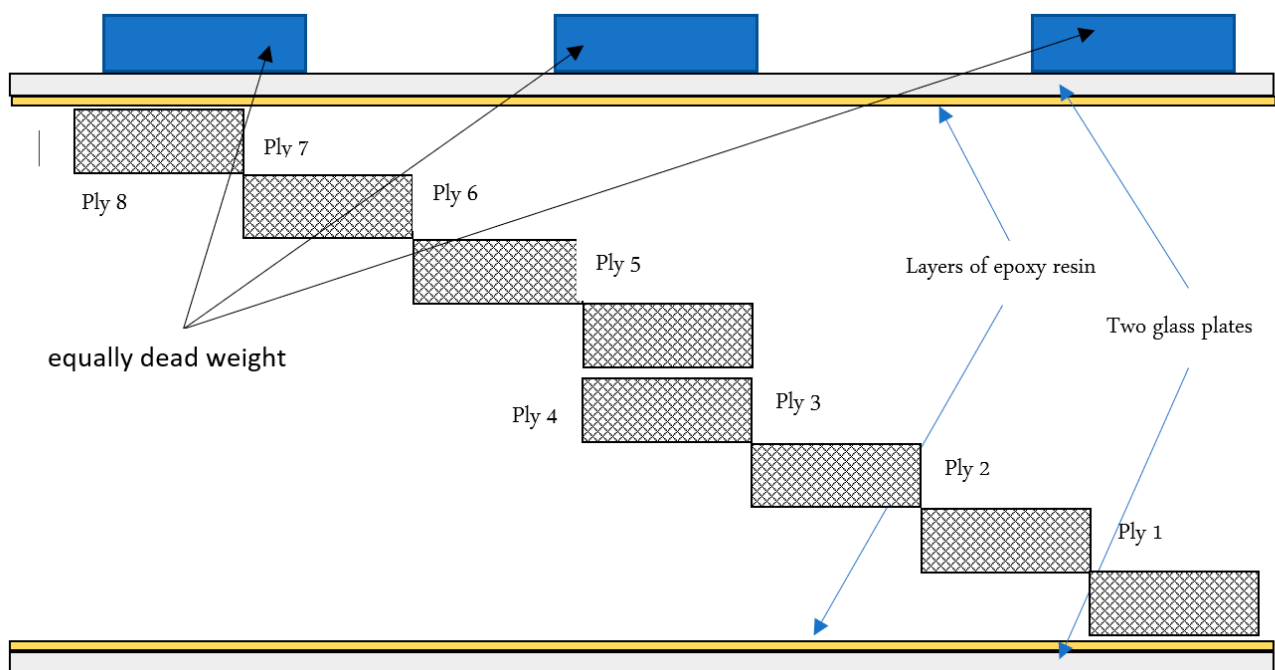
Figure 3. Schematic drawing of laminate setup.

3.2. Un-Notch Tensile Test

The un-notch tensile test was performed according to ASTM D3039 [57]. The test is performed on CFRP, GFRP and RGFRP to determine the mechanical properties. The tests were carried out with H-series hydraulic materials testing machines (Zwick/Roell type: Z600H) [58] with a maximum load capacity of 600 kN at a control speed of 2 mm/min. The schematic representation of the specimen geometry can be seen in Figure 4a. The aluminium taps are placed at both ends of the specimens in the clamping area to prevent slippage and damage to the specimens under the action of the clamping force. Real photos of glass-fibre-reinforced epoxy laminates are shown in Figure 4b.

(a)

(b)
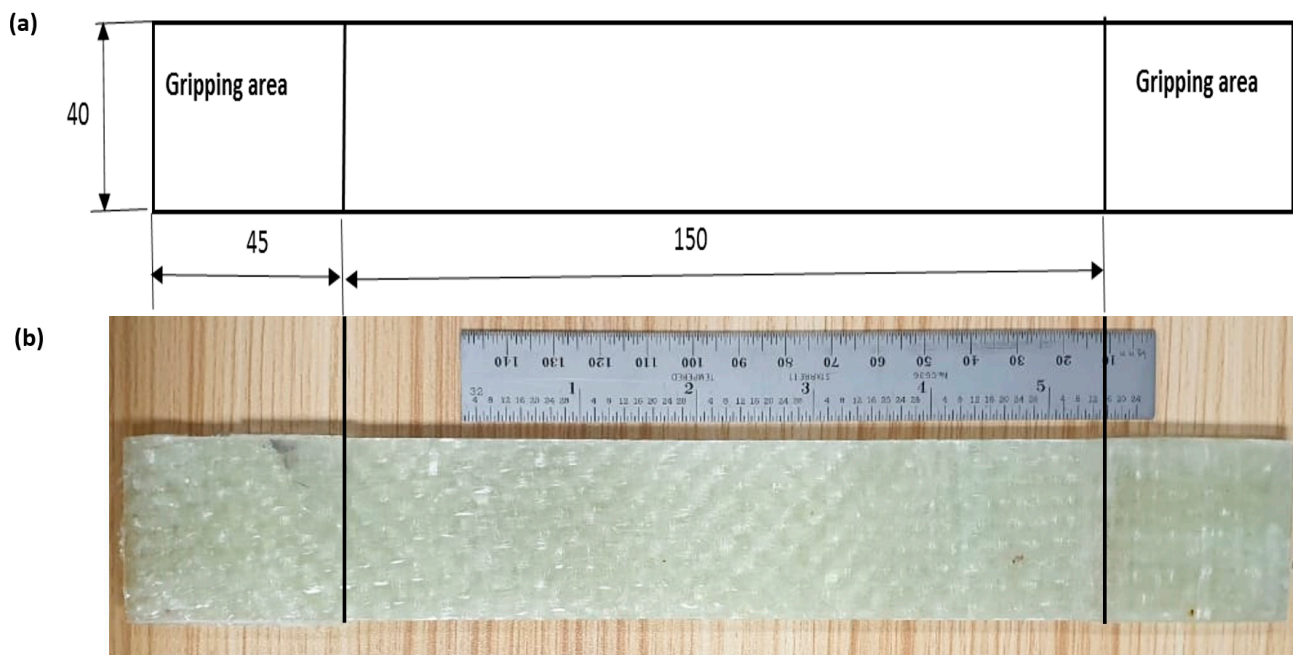
Figure 4. Tensile test specimen geometry; (**a**) Schematic drawing (dimensions in mm); (**b**) Real image.

3.3. Centre Notch Test

There are many standards for fracture toughness testing based on concepts of linear elastic fracture mechanics to determine the crack tip. The simplest standard based on the model developed by Soutis and Flick [11] is the central notch specimen tensile test. It has been recommended for multidirectional composite laminates. The procedures consist of measuring the peak load at crack propagation of a certain value of the precrack, then the remote failure stress σ_p is measured. Then, the fracture toughness K_{IC} is calculated using Equation (7) as follows [50]:

$$K_{IC} = \sigma_p \times \sqrt{\pi a} \sqrt{sec\left(\frac{\pi a}{w}\right)} \tag{7}$$

In addition to the corresponding surface release energy (G_{IC}) can be calculated by Equation (8) as follows:

$$G_{IC} = \frac{K_{IC}}{E_{eq}} \tag{8}$$

The notch must be machined with a cutter or diamond saw and a crack must be made in the centre of the specimen by tapping or sawing with a fine razor blade. See the sample geometry and dimensions in Figure 5. Five samples with a width of 45 mm and a central crack of 15 mm were used for the test matrix. The specimen geometry and dimensions (see Figure 5a) can be produced with a quartz disc saw. Five specimens with a width of 45 mm and a central crack of 15 mm with an approximation width of 3 mm, as recommended by Soutis and Flick [11], were used for the test matrix. The measurement height was chosen to be 90 mm according to J.C. Newman & and M. Jordan Haines [59] (see Figure 5b). Aluminium taps were placed in the clamping area to prevent damage to the machine jaws. The tensile test was carried out with a computerised universal testing machine (Zwick/Roell type: Z600H) [58] with a maximum load capacity of 600 kN at a control speed of 2 mm/min, with both load and displacement recorded by computer during the test.
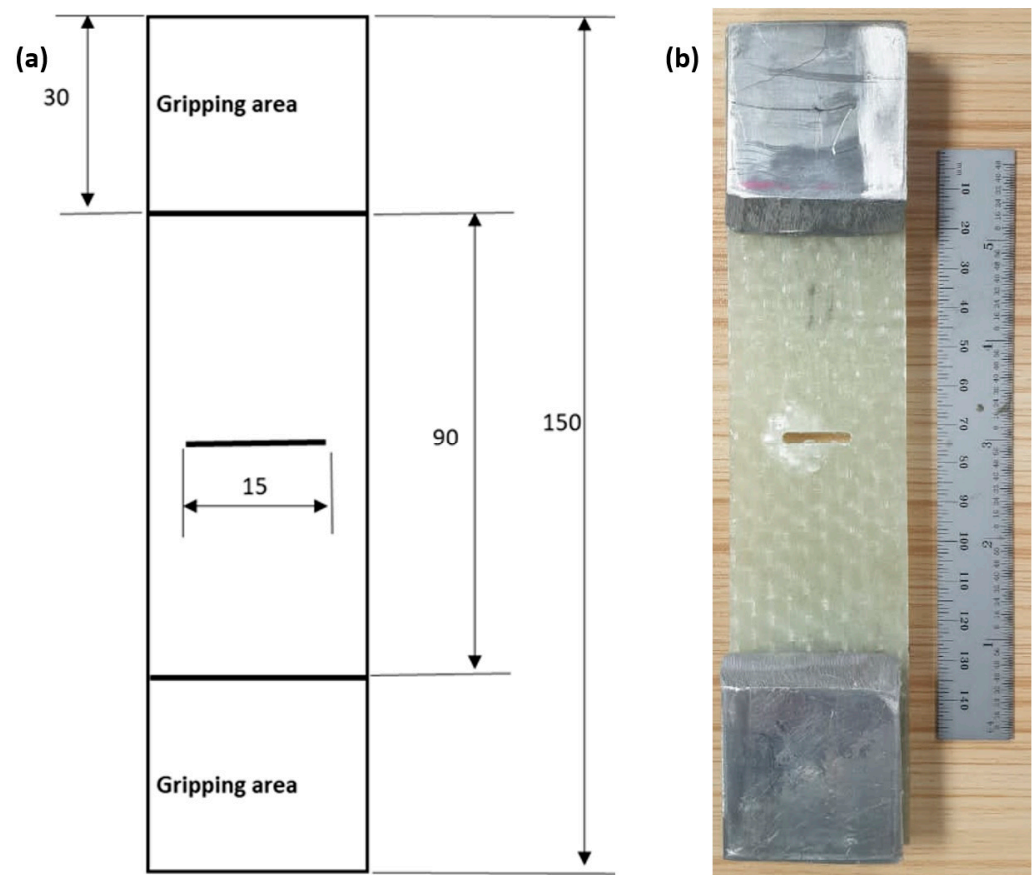
Figure 5. Centre notch tension specimen. (**a**) Schematic drawing (dim. in mm); (**b**) Real image.

3.4. Extended Finite Element Method XFEM

The XFEM was proposed by Belytschko and Blak [60] based on the work of Melenk and Babuska [61]. It is characterised by neglecting the need to modify the mesh as the crack progresses [62]. Therefore, the analysis of fracture toughness and stress intensity factor can be performed in a shorter time while the crack propagates with considerable accuracy [63]. Therefore, it enables crack modelling independently from the mesh. In XFEM, the finite element unit and the enhancement function (Equation (10)) are divided as follows [62]:

$$u^h = \sum_{i \in I} u_i N_i(x) + \sum_{i \in I} a_i N_i H(x) + \sum_{i \in k1} N_i(x) \left(\sum_{l=1}^{4} b_{i,1}^l F_1^l(x) \right)$$
$$+ \sum_{i \in k2} N_i(x) \left(\sum_{l=1}^{4} b_{i,1}^l F_2^l(x) \right) \tag{9}$$

where l is the node in the mesh, u_i is degree of freedom, N_i is shape function related to node i, a_i is node crack length, ($i \in I$) is the subset of nodes enriched by the Heaviside function $H(x)$, ($i \in k1$) and ($i \in k2$) are the set of nodes to enrich to model crack tips numbered 1 and 2, respectively, and $b_{i,1}^l$, $b_{i,2}^l$ are degrees of freedom of node 1 and 2. While the asymptotic crack-tip functions $F_2^l(x)$ can be calculated using Equation (11) as follows:

$$F_2^l(x) = \left\{ \sqrt{r} \sin\left(\frac{\theta}{2}\right), \sqrt{r} \cos\left(\frac{\theta}{2}\right), \sqrt{r} \sin\left(\frac{\theta}{2}\right) \sin(\theta), \sqrt{r} \cos\left(\frac{\theta}{2}\right) \sin\theta \right\} \tag{10}$$

Each function in these equations has its role in predicting the fracture toughness and stress intensity factor. The work is carried out over the mean notch of the specimen to simulate the fracture toughness or the corresponding surface release energy (G_{IC}), but

according to LEFM the simulation measures the J-integral around the crack tip from the problem of singularities of the radius $\sqrt{r}$.

XFEM Extraction

The model was created with ABAQUS 6.11, a commercial software. The finite element domain is shown in Figure 6a, while the mesh and load domains are shown in Figure 6b. It is a rectangular plate with dimensions 90 mm $\times$ 45 $\times$ thickness, which are 2.5 mm for S1, 5 mm for S2 and 4 mm for S3 (see Figure 6a). In XFEM, a stationary crack was used to measure five J-integrals around the crack tops. The crack was created and inserted in the central zone A as a straight, plane strand of 15 mm length with the same specimen thickness. The initial geometry of the specimens and the initial shape of the precrack or crack length had no effect on the fracture toughness for stationary cracks as reported in [11,64,65], which reduces the number of specimens needed (only one crack length of the specimen is used). This form is preferable in FEM as the strain field around the crack tip becomes singular and the singularity improves the accuracy of the analyses. In addition, 1650 C3D8R elements with a global size of 4.5 were used. The shape of the hexagonal elements was chosen using the swept meshing technique to create a more accurate and dense mesh. The mesh in area A was finer than that of the other plate areas with a global size of 0.9. Three mesh sizes were investigated to obtain an optimal mesh size: 930 (A), 990 (B) and 1650 (C) elements. The initial boundary conditions were a displacement control that completely restricted the movement in all directions at the lower end, while allowing it to move in the y-direction at the upper end. The longitudinal load (F) was applied through the upper ends (see Figure 6c). The load was chosen according to the maximum failure load suggested by the experimental results of CNT. It was 16.5 kN, 29 kN and 10.2 kN for S1, S2 and S3 materials, respectively. The damage criterion was the maximum principal stress (Maxps) theory. Therefore, the maximum principal stress of an un-notch tensile strength was 303 MPa, 187.5 MPa and 125 MPa for materials S1, S2 and S3, respectively. The maximum traction displacement was chosen as the criterion for damage development. At this stage, it was the maximum crack opening δ_{cr} at which the maximum stress was evident. Therefore, the model extracted by Hahn and Rosenfiled [66] and Perez [67] was selected to calculate the critical crack opening δ_{cr} using Equation (12) as [68] follows:

$$\delta_{cr} = t \times \varepsilon_f \tag{11}$$

The woven fabric composite laminates are commonly simulated using isotropic elastic with longitudinal young modulus of 27.13 GPa, 15.36 GPa and 5.01 GPa for S1, S2 and S3 materials, respectively, whereas a passion ratio equally considers all materials and was selected as 0.34. The materials used in the XFEM are listed in Table 2, these materials were obtained from the simple tension test. In addition, the XFE models can be surmised Additionally, in Table 2, the core subroutine of the code was illustrated in the Appendix A.

Table 2. All XFE model parameters and materials.

Material	Young Modulus (GPa)	Tensile Strength, (MPa)	Passion Ratio [69]	Applied Load (B.C) kN	Element Type	Number of Elements	Evolution Dis. δ_{cr}
CFRP (S1)	27.13	303	0.34	16.5	C3D8R	1650	0.03
GFRP-w (S2)	15.36	187.5	0.34	29	C3D8R	1650	0.125
GFRP-R (S3)	501	125	0.34	10.2	C3D8R	1650	0.03
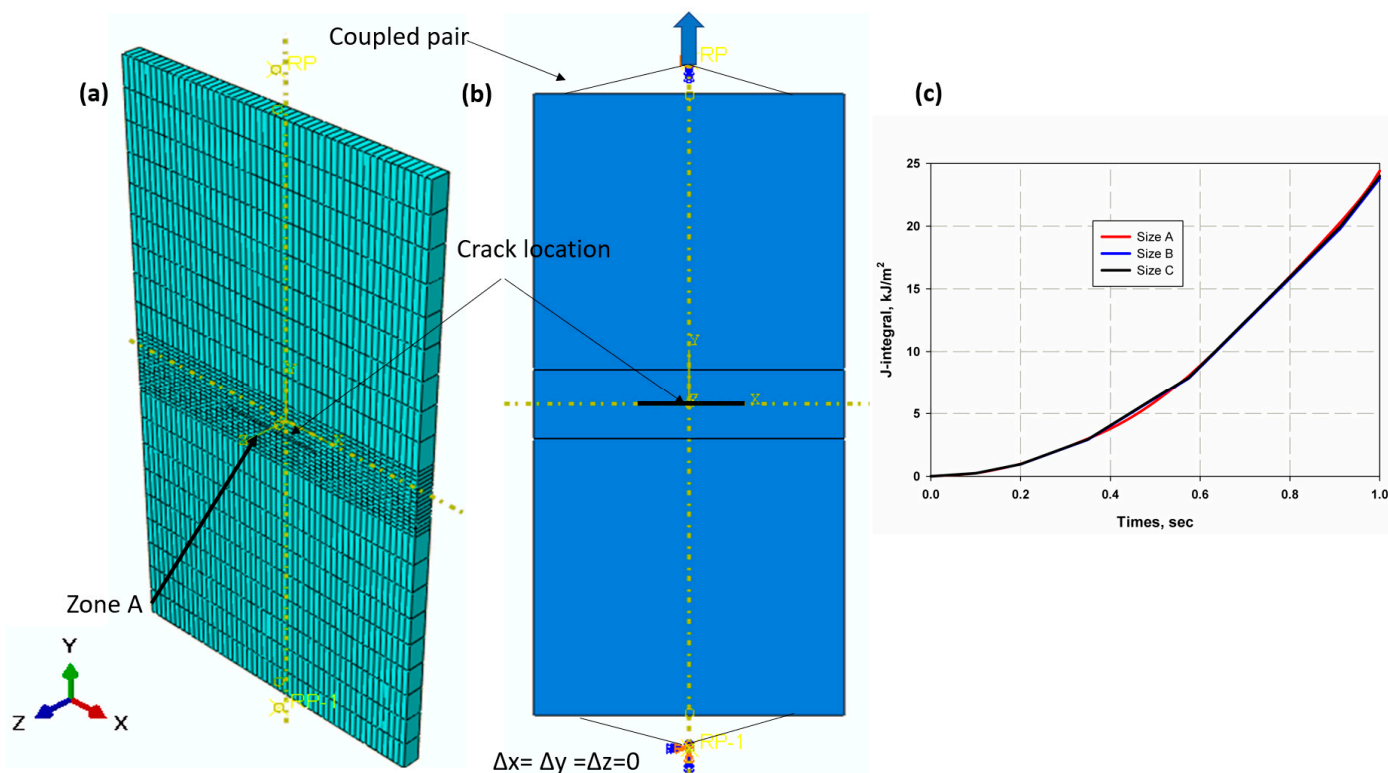
Figure 6. XFEM domain (**a**) mesh, (**b**) boundary condition and (**c**) mesh convergence.

3.5. Essential Work of Fracture Test

The essential work of the fracture testing methodology was carried out using a DENT specimen with an average width of 40 mm, as described in [12,70] (see Figure 7). The specimen DENT was selected according to the recommendations of [42,71–73]. The chosen shape helps to prevent buckling due to symmetry, as the buckling effect is not acceptable as it leads to a large decrease in the tensile load. The tensile load is applied to both ends of the specimens until complete failure. The tensile load is applied at a controlled crosshead speed of 2 mm/min according to [44]. The central crack is created with a 1 mm-thick steel saw disc. The material has a width of 40 mm and a thickness of 2 mm for the S1 and S3 specimens and 5 mm for the S2 specimens. Five specimens were used for EWF values according to the recommendations of [74] for different strip lengths of 4, 8, 12, 16 and 20 mm at room temperature. The mechanical work W under the load–displacement curve would be calculated as follows:

$$W_f = \int_0^\delta p \, d\delta \tag{12}$$

where δ are displacements at failure, respectively, and p is the applied load. The obtained total energy W_f (measured using Equation (4)) was plotted against ligament length L.
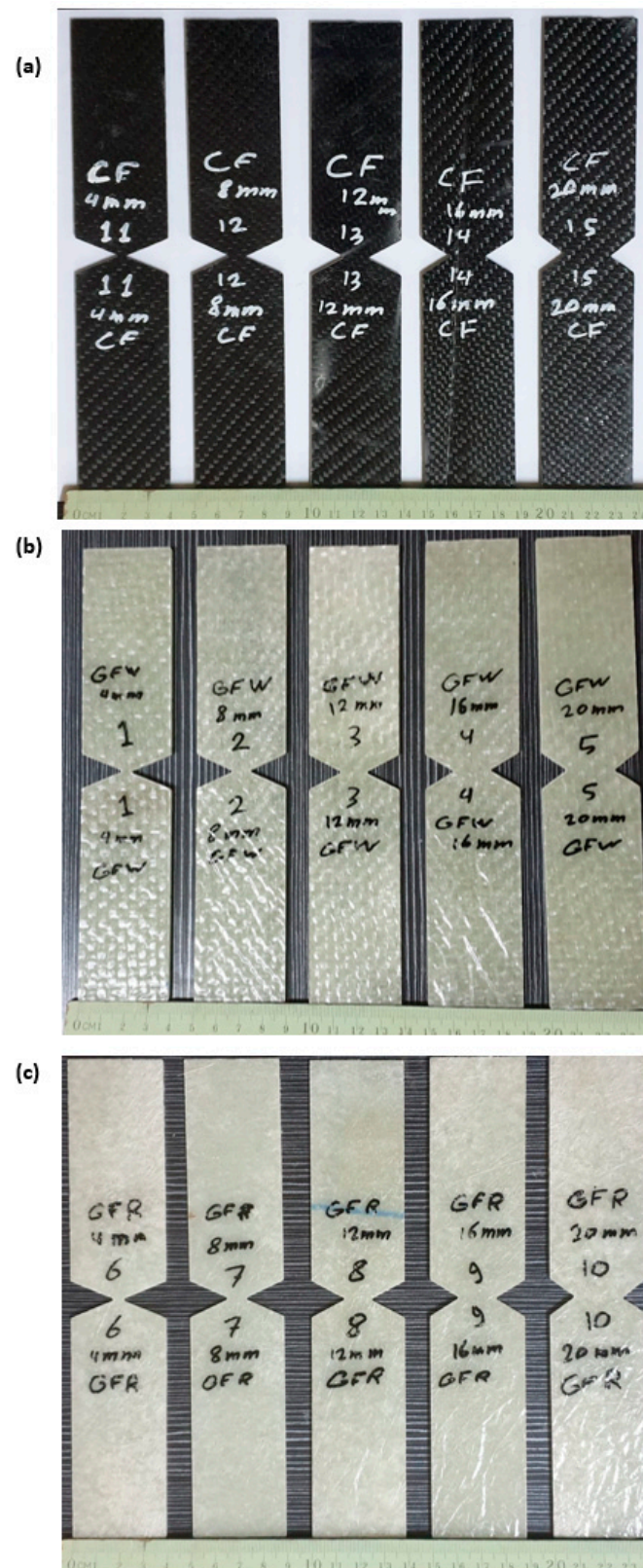
Figure 7. Ideal image of EWF specimens (**a**) CFRP (s1), (**b**) GFRP-w (s2) and (**c**) GFRP-W(s3).

4. Results and Discussion

Figure 6c shows the relationship between the J-integral and time. It can be seen that for an elastic XFEM model for a stationary crack, the mesh refinement has less influence. The

convergence of the mesh has been studied in many papers [4,33,63] and is not significantly affected in the simulation with XFEM, which is a great advantage. Therefore, it was not necessary to investigate the accuracy of the convergence of the mesh in a complex way. The stress–strain relationship of the composite laminates is shown in Figure 8. It was found that S1 of CFRP has an increasing average strength of 303 MPa with a standard deviation SDV 17.98 MPa and a modulus of elasticity of 27.13 GPa with SDV 1.7 GPa, corresponding to (GFRP-W) a lower average tensile strength of 187.5 MPa with SDV 10.5 MPa for GFRP S2 and a modulus of elasticity of 15.36 GPa with SDV of 1.19 GPa, despite the lower values in the case of GFRP-R S3, where the average tensile strength decreased to 125 MPa with SDV of 2.5 MPa and the corresponding modulus of elasticity was very low at 5.01 GPa with SDV of 1.5 GPa. This is due to the fact that carbon fibres have higher stiffness and strength than woven glass fibres or even random fibres. The percent elongation of material S3 with random fibre (GFRP-R) is almost 2.43 larger than that of material S1 with carbon fibre (CFRP), which is due to the fact that carbon fibre has higher stiffness and lower ductility, while material S3 with woven glass fibre has intermediate percent elongation values. The failure modes show net stress for both S1 and S2 (see Figure 9a,c), while for the S1 material with carbon fibres, a straight crack path is observed with fibre breakage at the crack surfaces, while for the S3 material with disordered fibre direction, the net stress is associated with fibre pull-out because the fibres have many directions and possibly due to the lower adhesion between the disordered glass fibres compared to carbon fibres. In addition, the S2 material with woven glass fibres has no failure zone (see Figure 9b) because the failure occurs in the thickness as delamination, which is due to the relative increase of 5 mm in thickness compared to other materials.
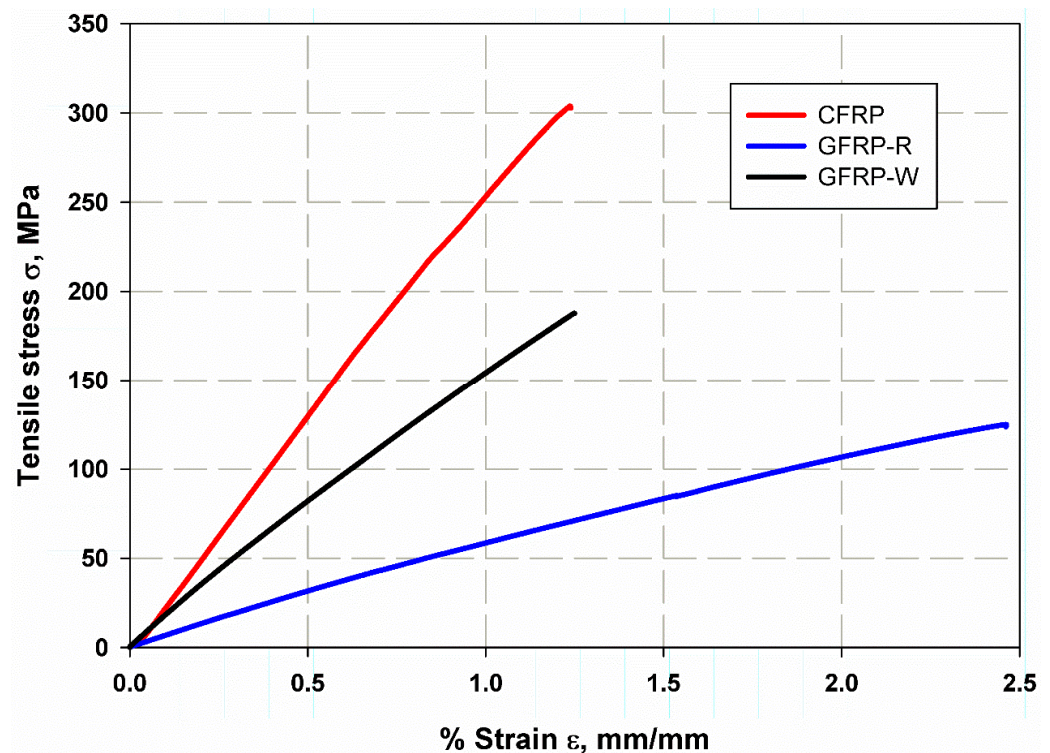
Figure 8. Stress and strain relation for un-notch tensile strength of composite laminates.
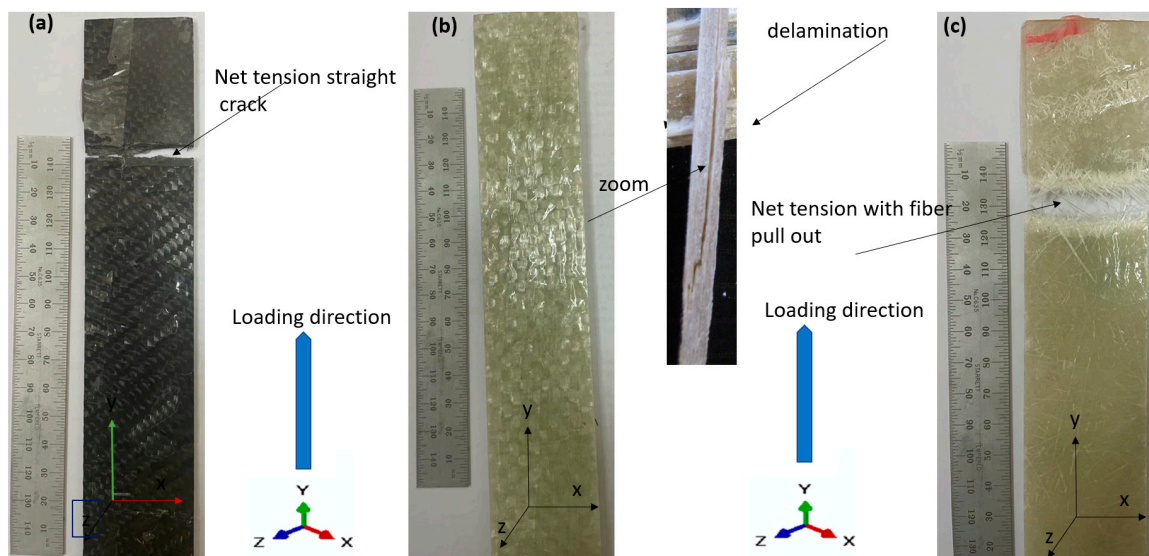
Figure 9. Modes of failure (**a**) CFRP, (**b**) GFRP-W and (**c**) GFRP-R.

4.1. Centre Notch

The relationship between load and displacement was shown in Figure 10 for the tensile test on a specimen with a medium notch. The CFRP specimens show a brittle behaviour with a very small softening range, while this was relatively larger for GFRP-R or GFRP-W. This is due to the greater thickness of GFRP-R and GFRP-W compared to the thickness of CFRP, which increases the cross-sectional area. The 5% odorous load PQ would be more suitable for calculating the maximum crack propagation stress σ_p. The average values were 146.5 MPa with SDV 6.17 MPa, 128.6 with SDV 5.6 MPa and 56.11 MPa with SDV 4.4 MPa for CFRP, GFRP-W and GFRP-R, respectively. By substituting these stresses into Equations (7) and (8), you can measure both the fracture toughness K_{IC} and the surface energy (G_{IC}). The average values of (G_{IC}) were therefore 25.15 kJ/m², 32.5 kJ/m² and 20.22 kJ/m² for GFRP-W and GFRP-R, respectively. The failure modes are shown in Figure 11. All specimens were net stress (see Figure 11a,c), but due to the greater thickness of GFRP-W, the failure mode delamination was observed (see Figure 11b).
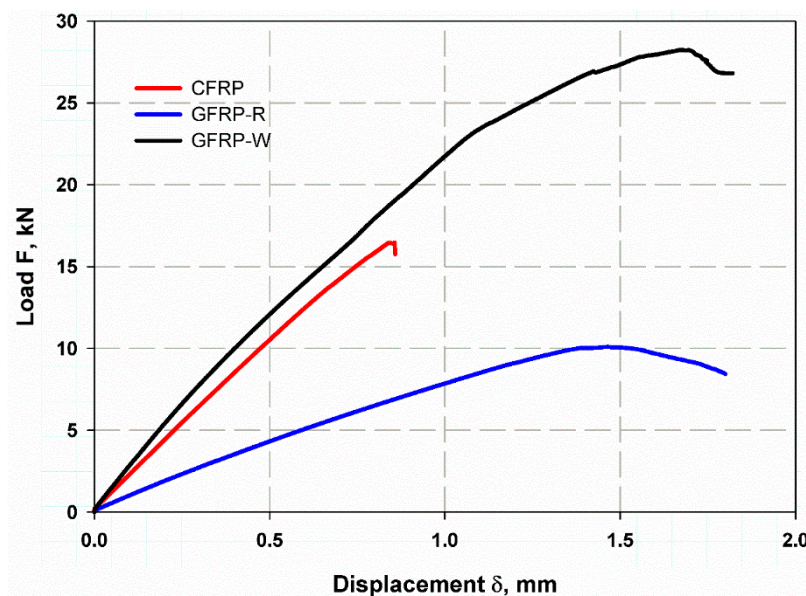
Figure 10. Load and displacement curve of CNT.
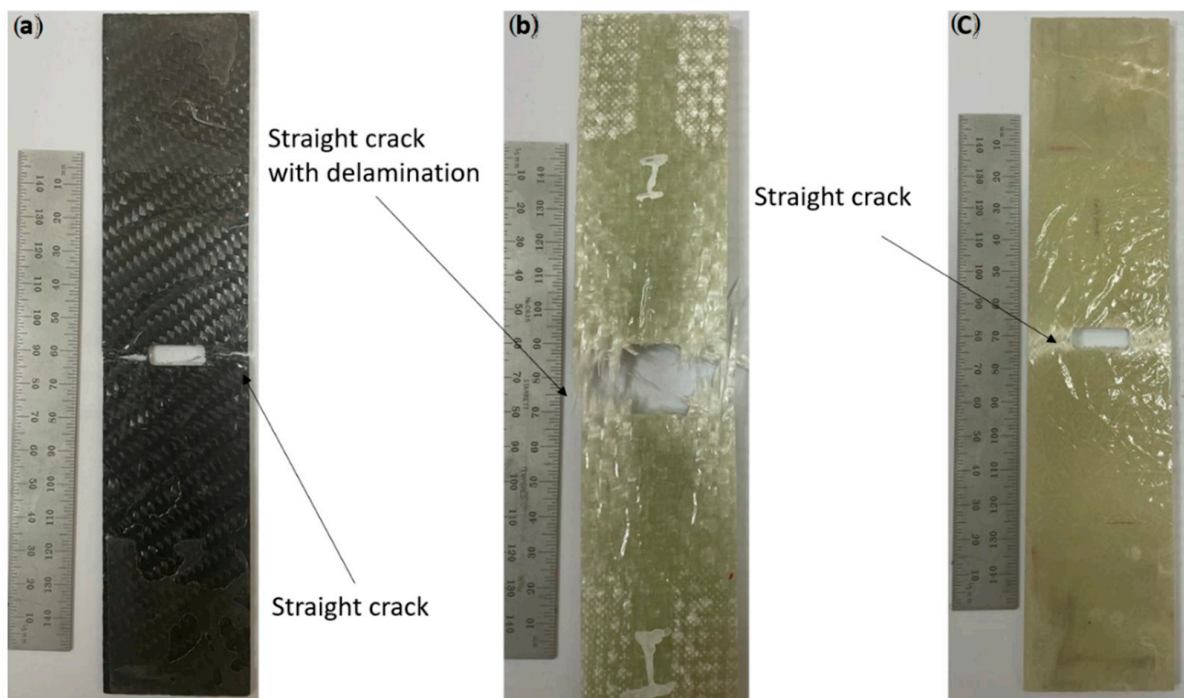
Figure 11. Modes of failure in CNT (**a**) CFRP, (**b**) GFRP-W and (**c**) GFRP-R.

4.2. Essential Work of Fracture Approach

The relationship between load and displacement for the essential fracture work EWF is shown in Figure 12a–c for one sample each of CFRP, GFRP-W and GFRP-R. The total work carried out (W_f) is measured (Equation (9)) as the area under the curves and then divided by the ligament area (Lt) to obtain the total energy per area (W_f) using Equation (3). Therefore, the essential work of fracture *(we)* was presented in the linear regression of Figure 13. The essential work *(we)* was 24.93 kJ/m² with an SDV of 3.6 kJ/m², 34.28 kJ/m² with an SDV of 3.4 kJ/m² and 19.28 kJ/m² with an SDV of 3 kJ/m² for CFRP, GFRP-W and GFRP-R, respectively. As reported by [42], to ensure linear regression, the ligament length should not be less than 3–5 times the plate thickness. Therefore, the ligament lengths used to calculate the EWF vary according to the thickness of the samples. If we return to Figure 13, we see that the softening zone, which is responsible for the part of the non-essential fracture work, is relatively small. As mentioned earlier, for quasi-brittle materials such as composites, the plastic zone before the crack tip lies between brittle material (linear material) and ductile material (non-linear material). The slope of each line in Figure 14 illustrates the plastic (softening) part or the non-essential work. It has higher values of 95.5 for GFRP-R than for other materials and a lower value of 3.3 for CFRP, while the intermediate value is 17.38 for GFRP-W. The failure modes are shown in Figure 14A–C. Net stress with straight crack surface without delamination affected CFRP and GFRP-R (see Figure 14A,C), but delamination was observed through the thickness of GFRP-W specimens (see Figure 14B), which is due to their relatively larger thickness. In addition, fibres were pulled out from the GFRP-W and GFRP-R specimens, while fibre breakage was observed in CFRP, which can be attributed to the relatively high stiffness and good debonding ability between carbon fibres and epoxy resin. Table 3 listed all maximum forces and corresponding stresses for all tested specimens and it was shown that the maximum stress values were for specimens S3.
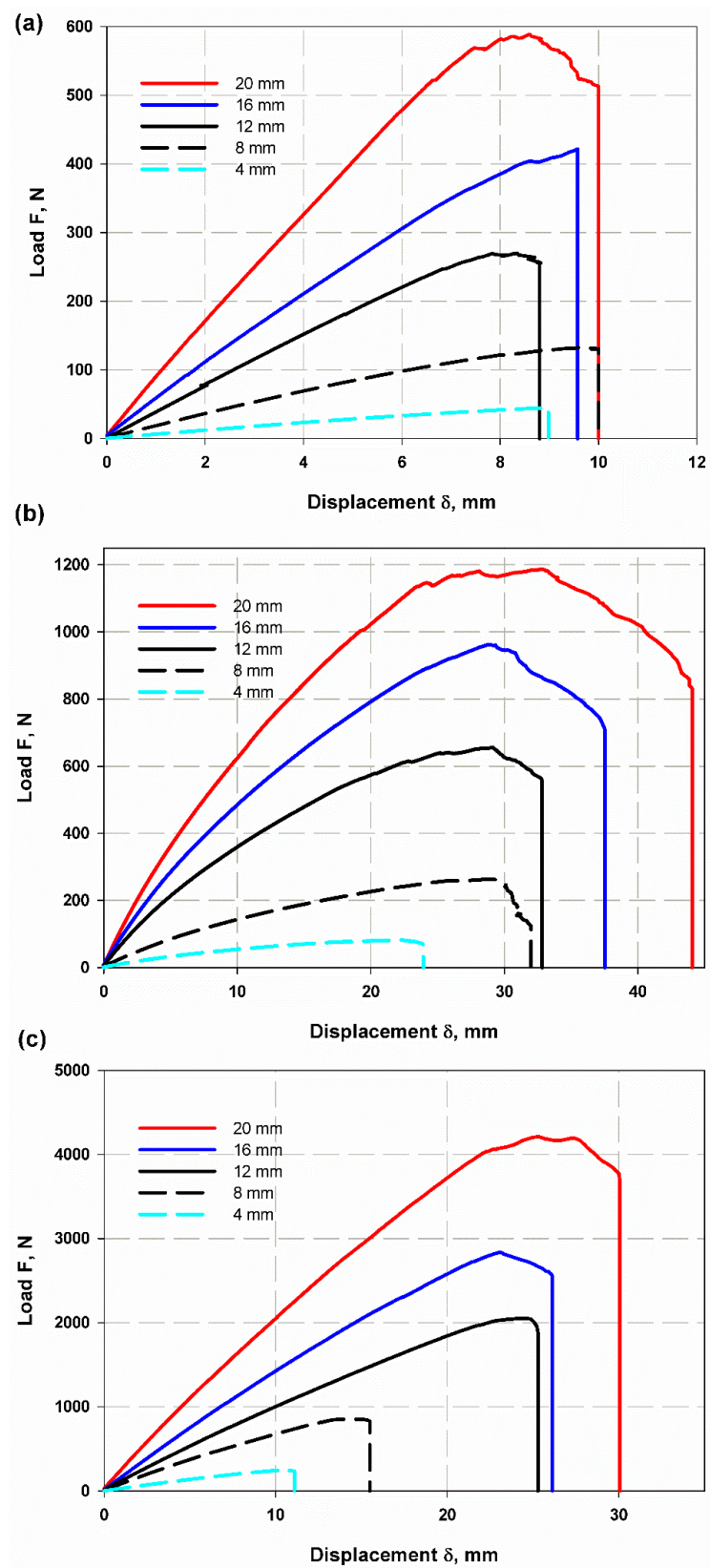
Figure 12. Load and displacement curve in EWF (**a**) CFRP, (**b**) GFRP-W and (**c**) GFRP-R.
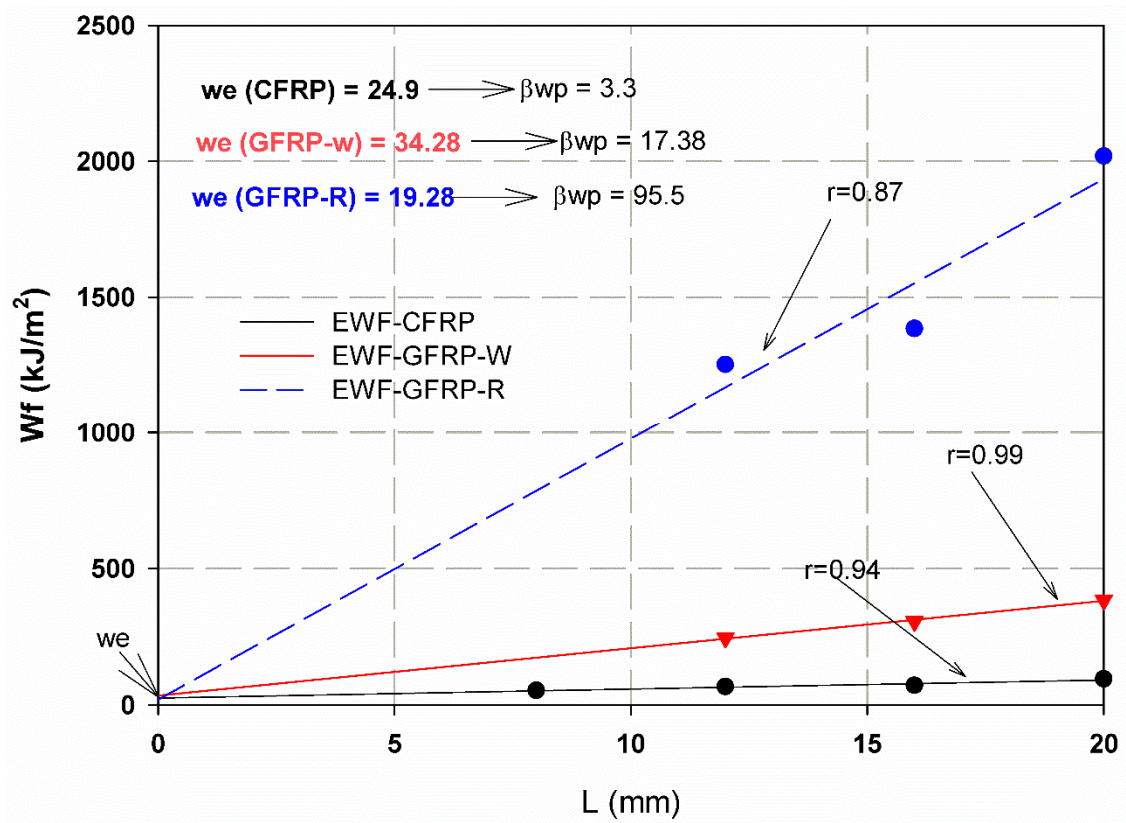
Figure 13. Energy and ligament relation for EWF approach.

(**A**)
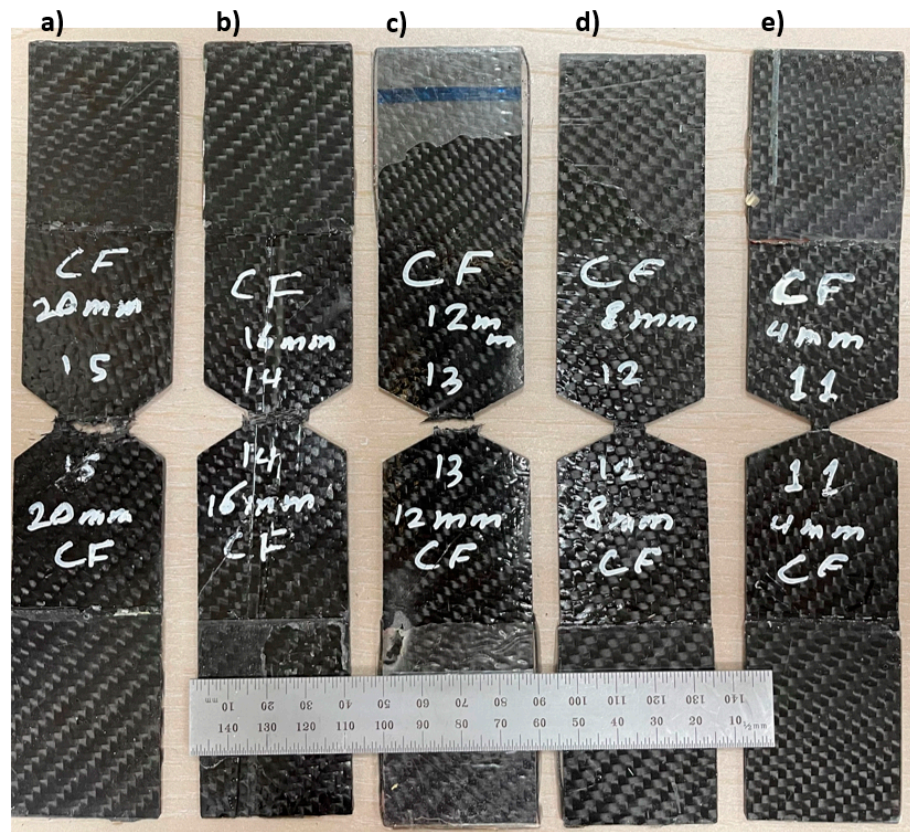
Figure 14. *Cont*.
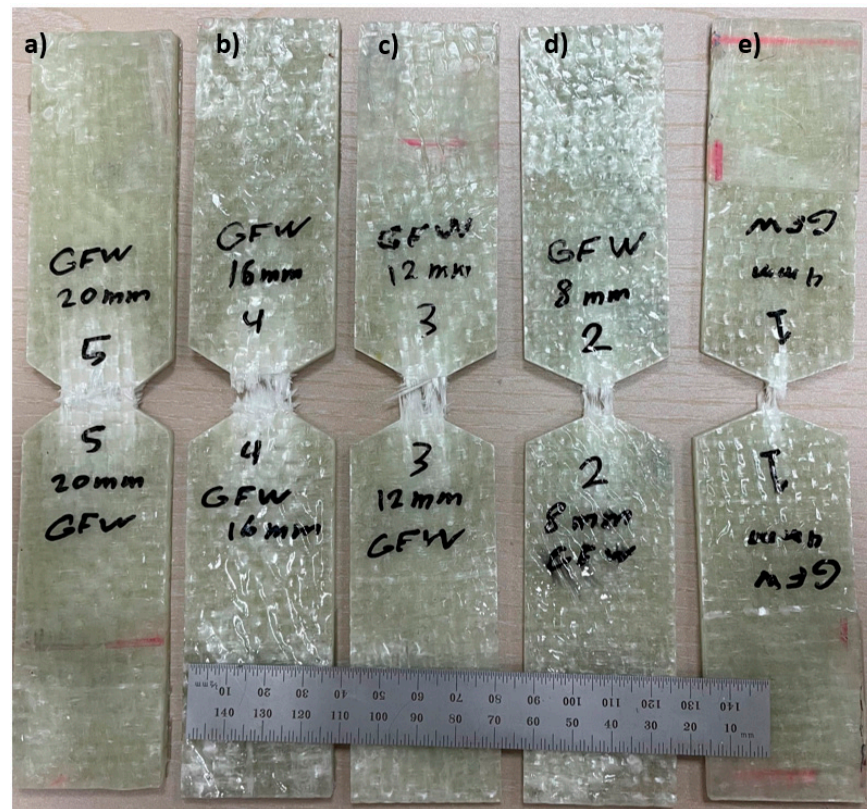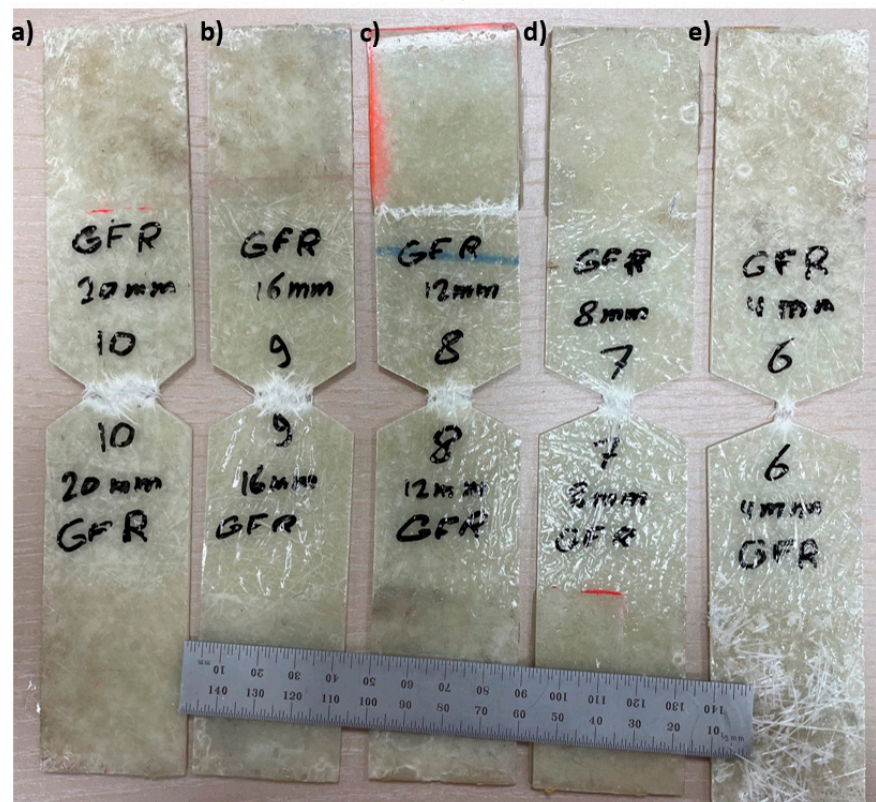
Figure 14. (**A**) Failure modes in EWF test of CFRP: (**a**) 20 mm, (**b**) 16 mm, (**c**) 12 mm, (**d**) 8 mm and (**e**) 4 mm. (**B**) Failure modes in EWF test of GFRP-W: (**a**) 20 mm, (**b**) 16 mm, (**c**) 12 mm, (**d**) 8 mm and (**e**) 4 mm. (**C**) Failure modes in EWF test of GFRP-R: (**a**) 20 mm, (**b**) 16 mm, (**c**) 12 mm, (**d**) 8 mm and (**e**) 4 mm.

Table 3. Comparing the double edge notch specimens with each ligament length.

Specimens	Load (kN)					Stress (MPa)				
Ligament length (mm)	4	8	12	16	20	4	8	12	16	20
CFRP (s1)	39	134	267	418	585	0.48	1.66	3.34	5.225	7.313
GFRP-W (s2)	82	257	644	962	1171	0.41	1.29	3.22	4.81	5.85
GFRP-R (s3)	244	853	2028	2835	4205	3.26	3.05	10.66	25.35	35.44

4.3. Comparison between Methods

The EWF data agree well with the data of the standard ASTM fracture toughness test specimens. To obtain satisfactory results, the XFEM results for the CNT specimens were also used (see Table 4). Figure 15 shows the comparison between the three models. It was also found that the XFEM is robust and good at predicting the fracture toughness of the different woven fibre laminates, with a lower percentage error of 4.65%, 2.97% and 5.25 % for CFRP, GFRP-W and GFRP-R, respectively. Moreover, it was clearly observed that the percentage error was very close when comparing the EWF with the experimental results of the CNT samples, namely 0.83%, 5.16% and 4.64% for CFRP, GFRP-W and GFRP-R, respectively. The average percentage EWF error for CFRP was the lowest at 0.83, which can be attributed to the fact that the lower thickness and high stiffness reduces the softening zone and also reduces the overall effect per area (see Figure 12a). The lowest percentage error of 2.97 was for GFRP-W when XFEM was implemented, as XFEM was based on the initial load introduced in the model subroutine. It was also found that the EWF method is applicable for measuring the fracture toughness of composite laminates. This method is characterised by its simplicity and does not depend on LEFM, where the problem of singularities, crack tips and other geometry factors can affect the accuracy of the results. In addition, the CNT specimens and other standard specimen geometries based on LEFM, such as compact stresses, require special equipment and relatively expensive preparation sequences and procedures. Furthermore, the difference between the fracture toughness of S1 and S2 was found to be almost 28% and between S1 and S3 almost 20%. The S2 material has higher values for fracture toughness than S2 and S3, which is due to a higher amount of epoxy resin than the other samples, although the damage mode delamination by these types of material is not preferred.

Table 4. Comparison between fracture toughness measured using CNT, XFEM and EWF.

Material Type	Fracture Toughness, G_{IC}, kJ/m^2 (CNT)	Fracture Toughness, G_{IC}, kJ/m^2 (XFEM)	% Error	Fracture Toughness, we, kJ/m^2 (EWF)	% Error
CFRP (s1)	25.14	23.97	4.65	24.936	0.83
GFRP-W (s2)	32.59	31.62	2.97	34.28	5.16
GFRP-R (s3)	20.22	19.16	5.25	19.28	4.64
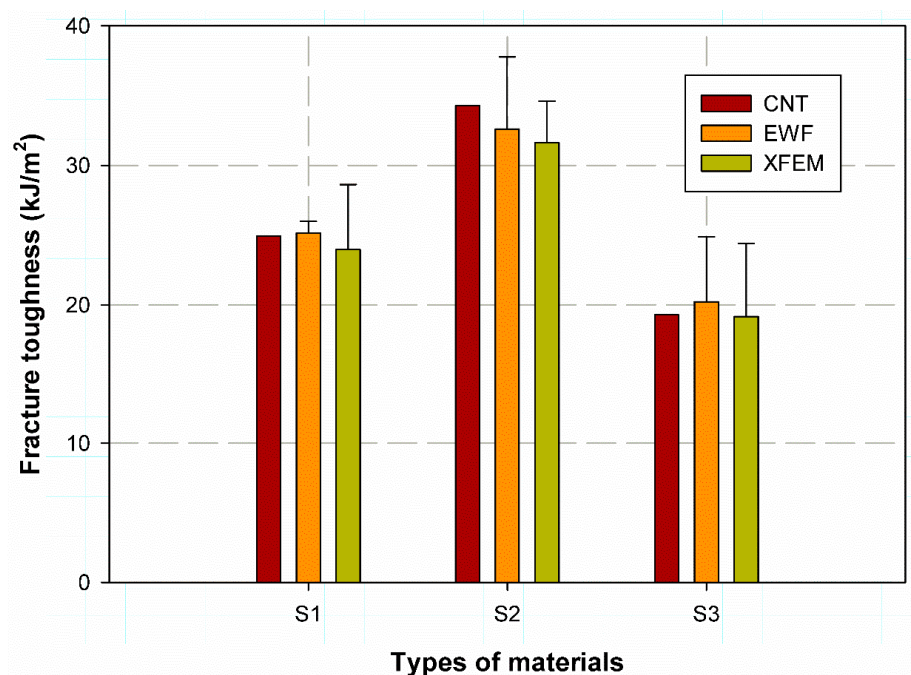
Figure 15. Comparison of EWF with other methods.

5. Conclusions

Fabric-reinforced epoxy laminates have more competitive properties as a quasi-brittle material than other multidirectional composite laminates with the same fibre types. This is due to their relatively symmetrical properties. The fracture toughness of the three fabric laminates CFRP, GFRP-W and GFRP-R was measured to be 25.14 kJ/m^2, 32.59 kJ/m^2 and 20.22 kJ/m^2, respectively. The EWF assessment was found to be applicable to these types of brittle material with a small plasticity zone in front of the crack tips. The average accuracy of the method was 3.54% compared to a standard CNT specimen shape and 4.5% compared to the numerical concepts of the XFEM method. In conclusion, it was reported that EWF evaluation can be considered a standardised technique for woven quasi-brittle material. This study can be extended to metal matrix composites and sandwich laminates; moreover, simulation with FEM can include the main fracture concepts to predict the numerical values of EWF. The EWF can also be compared to other standard geometries used in measuring fracture toughness to provide a valuable table for a variety of geometries and materials. Despite these advantages, there are limitations to the use of this method, such as the relationship between strip length and thickness, the accuracy of the fitting regression and the effect of sample size on fracture toughness.

Author Contributions: Conceptualization, M.Y.A., M.K.H. and S.A.A.; methodology, M.Y.A. and S.A.A.; software, M.Y.A. and M.K.H.; validation, A.-R.Z. and M.K.H.; formal analysis, M.Y.A., M.K.H. and A.-R.Z.; investigation, M.Y.A., M.K.H. and S.A.A.; resources, A.-R.Z.; writing—original draft preparation, M.Y.A., M.K.H. and S.A.A.; writing—review and editing, M.Y.A. and S.A.A.; supervision, M.K.H. and M.Y.A.; project administration, M.Y.A. and A.-R.Z.; funding acquisition, A.-R.Z. All authors have read and agreed to the published version of the manuscript.

Institutional Review Board Statement: Not applicable.

Informed Consent Statement: Not applicable.

Data Availability Statement: The data presented in this study are available on request from the corresponding author.

Conflicts of Interest: The authors declare no conflict of interest.

Nomenclature

δ	Displacement at failure
βy	Geometric shape factors related to the plastic zone during ligament yielding
βp	Geometric shape factors related to the plastic zone during tearing after necking
βw_p	Slope of linear fitting regression
β	Plasticity shape factor
t	Thickness of the specimen
p	Applied load
$d\delta$	Displacement increment
L	Ligament length
a0	Pre-crack length
σ_u	Un-notched tensile strength
δ_o	0.2% offset displacement
w_y	Essential work of the fracture in the elastic zone
w_p	Non-essential work of the fracture
w_e	Essential work of the fracture
W_y	Elastic energy of the elastic and yielding ligament length
W_{py}	Relative energy in plastic and yielding of ligament length
W_{pp}	Relative plastic energy in tearing and necking
W_p	Energy of the tearing and necking of the plastic zone
W_f	Total strain energy attributed to the fracture
J_i	Initiation J-integral in EPFM
J_{CFE}	Finite element J-integral
J_C	Critical J-integral or release energy in elastic plastic fracture mechanics (EPFM)
G_o	Initiation surface release energy in LEFM or crack initiation resistance
G_{IC}	Surface release energy or critical mode I fracture toughness

Appendix A

The XFEM input files

```
**PARTS
*Preprint, echo=NO, model=NO, history=NO, contact=NO
**PARTS
*Part, name = Part-1
*Element, type=C3D8R
* *Nset, nset=Part-1-RefPt_, internal
*Nset, nset=Set-1
*Surface, type=ELEMENT, name=Surf-1
*Surface, type=ELEMENT, name=Surf-2
** Section: Section-1
*Solid Section, elset=_PickedSet15, material=Material-1
*End Part
*Part, name=crack
*End Part
** ASSEMBLY
*Assembly, name=Assembly
*Instance, name = Part-1-1, part= Part-1
*End Instance
*Instance, name = Part-2-1, part= Part-2
*End Instance
** Constraint: Constraint-1
*Coupling, constraint name=Constraint-1, ref node=_PickedSet12, surface= Part-1
*Kinematic -1.Surf-1
```

```
** Constraint: Constraint-2
*Coupling, constraint name=Constraint-2, ref node=_PickedSet16, surface= Part-1-1.Surf-2
*Kinematic
*Enrichment, name=Crack-1, type=STATIONARY CRACK, elset=_PickedSet19
*End Assembly
** MATERIALS
*Material, name=Material-1
*Damage Initiation, criterion=MAXPS
303.,
*Damage Evolution, type=DISPLACEMENT
0.01,
*Density
1.5e-09,
*Elastic
27130., 0.3
Part-1-1.443, 3,Crack-1, -0.335333
Part-1-1.443, 4,Crack-1, -0.335333
Part-1-1.443, 5,Crack-1, 0.335333
Part-1-1.443, 6,Crack-1, 0.335333
Part-1-1.443, 7,Crack-1, -0.335333
Part-1-1.443, 8,Crack-1, -0.335333
Part-1-1.458, 1,Crack-1, 0.335333
Part-1-1.458, 2,Crack-1, 0.335333
Part-1-1.458, 3,Crack-1, -0.335333
Part-1-1.458, 4,Crack-1, -0.335333
Part-1-1.458, 5,Crack-1, 0.335333
Part-1-1.458, 6,Crack-1, 0.335333
Part-1-1.458, 7,Crack-1, -0.335333
Part-1-1.458, 8,Crack-1, -0.335333
Part-1-1.473, 1,Crack-1, 0.335333
Part-1-1.473, 2,Crack-1, 0.335333
Part-1-1.473, 3,Crack-1, -0.335333
Part-1-1.473, 4,Crack-1, -0.335333
Part-1-1.473, 5,Crack-1, 0.335333
Part-1-1.473, 6,Crack-1, 0.335333
Part-1-1.473, 7,Crack-1, -0.335333
Part-1-1.473, 8,Crack-1, -0.335333
Part-1-1.488, 1,Crack-1, 0.335333
Part-1-1.488, 2,Crack-1, 0.335333
Part-1-1.488, 3,Crack-1, -0.335333
Part-1-1.488, 4,Crack-1, -0.335333
** BOUNDARY CONDITIONS
** Name: BC-1 Type: Symmetry/Antisymmetry/Encastre
*Boundary
_PickedSet22, ENCASTRE
** _____
** STEP: Step-1
*Step, name=Step-1, inc=100000
*Static
1., 1., 1e-10, 1.
** BOUNDARY CONDITIONS
** Name: BC-2 Type: Displacement/Rotation
*Boundary
_PickedSet23, 1, 1
_PickedSet23, 3, 3
_PickedSet23, 5, 5
_PickedSet23, 6, 6
** LOADS
**
```

```
** Name: Load-1 Type: Concentrated force
*Cload
_PickedSet20, 2, 16500.
** CONTROLS
*Controls, reset
*Controls, parameters=time incrementation
, , 20, 20, 20, 20, 20, 20, , ,
** OUTPUT REQUESTS
*Restart, write, frequency=0
** FIELD OUTPUT: F-Output-1
*Output, field
*Node Output
CF, PHILSM, PSILSM, RF, U
*Element Output, directions=YES
LE, PE, PEEQ, PEMAG, S, STATUSXFEM
*Contact Output
CDISP, CSTRESS
*Output, history, frequency=0
** HISTORY OUTPUT: H-Output-1
*Contour Integral, crack name=Crack-1, contours=5, xfem
*End Step
```

References

1. Hassan, M.K.; Mohammed, Y.; Salem, T.; Hashem, A.M. Prediction of nominal strength of composite structure open hole specimen through cohesive laws. *Int. J. Mech. Mechatron. Eng.* **2012**, *12*, 1–9.
2. Bažant, Z.P.; Planas, J. *Fracture and Size Effect in Concrete and Other Quasibrittle Materials*; Routledge: New York, NY, USA, 2019.
3. Yu, C.; Lu, T. A damage-driven integration scheme in physically non-linear transient analysis for quasi-brittle materials. *Eng. Fract. Mech.* **2022**, *269*, 108531. [CrossRef]
4. Abdellah, M.Y. An approximate analytical model for modification of size effect law for open-hole composite structure under biaxial load. *Proc. Inst. Mech. Eng. Part C J. Mech. Eng. Sci.* **2020**, *235*, 3570–3583. [CrossRef]
5. Maio, L.; Fromme, P. On ultrasound propagation in composite laminates: Advances in numerical simulation. *Prog. Aerosp. Sci.* **2022**, *129*, 100791. [CrossRef]
6. Kalita, K.; Haldar, S.; Chakraborty, S. A Comprehensive Review on High-Fidelity and Metamodel-Based Optimization of Composite Laminates. *Arch. Comput. Methods Eng.* **2022**, *29*, 1–36. [CrossRef]
7. Sateesh, N.; Subbiah, R.; Nookaraju, B.; Nagaraju, D.S. Achieving safety and weight reduction in automobiles with the application of composite material. *Mater. Today Proc.* **2022**, *62*, 4469–4472. [CrossRef]
8. Anderson, T.L. *Fracture Mechanics: Fundamentals and Applications*; CRC Press: Boca Raton, FL, USA, 2017.
9. Catalanotti, G.; Camanho, P.; Xavier, J.; Dávila, C.; Marques, A. Measurement of resistance curves in the longitudinal failure of composites using digital image correlation. *Compos. Sci. Technol.* **2010**, *70*, 1986–1993. [CrossRef]
10. Dávila, C.G.; Rose, C.A.; Camanho, P. A procedure for superposing linear cohesive laws to represent multiple damage mechanisms in the fracture of composites. *Int. J. Fract.* **2009**, *158*, 211–223. [CrossRef]
11. Soutis, C.; Curtis, P.; Fleck, N. Compressive failure of notched carbon fibre composites. *Proc. R. Soc. Ser. A Math. Phys. Sci.* **1993**, *440*, 241–256.
12. Williams, J.; Rink, M. The standardisation of the EWF test. *Eng. Fract. Mech.* **2007**, *74*, 1009–1017. [CrossRef]
13. Cotterell, B.; Reddel, J.K. The essential work of plane stress ductile fracture. *Int. J. Fract.* **1977**, *13*, 267–277. [CrossRef]
14. Cotterell, B.; Atkins, A.G. A review of the J and I integrals and their implications for crack growth resistance and toughness in ductile fracture. *Int. J. Fract.* **1996**, *81*, 357–372. [CrossRef]
15. Rice, J.R. A Path Independent Integral and the Approximate Analysis of Strain Concentration by Notches and Cracks. *J. Appl. Mech.* **1968**, *35*, 379–386. [CrossRef]
16. Mai, Y.-W.; Powell, P. Essential work of fracture and j-integral measurements for ductile polymers. *J. Polym. Sci. Part B Polym. Phys.* **1991**, *29*, 785–793. [CrossRef]
17. Gobbi, G.; Colombo, C.; Vergani, L. Sensitivity analysis of a 2D cohesive model for hydrogen embrittlement of AISI 4130. *Eng. Fract. Mech.* **2016**, *167*, 101–111. [CrossRef]
18. Barany, T.; Czigány, T.; Karger-Kocsis, J. Application of the essential work of fracture (EWF) concept for polymers, related blends and composites: A review. *Prog. Polym. Sci.* **2010**, *35*, 1257–1287. [CrossRef]
19. Heidari, F.; Aghalari, M.; Tehran, A.C.; Shelesh-Nezhad, K. Study on the fluidity, mechanical and fracture behavior of ABS/TPU/CNT nanocomposites. *J. Thermoplast. Compos. Mater.* **2021**, *34*, 1037–1051. [CrossRef]
20. Clutton, E. *Essential Work of Fracture, in European Structural Integrity Society*; Elsevier: Berkeley, CA, USA, 2001; pp. 177–195.

21. Martinez, A.; Gamez-Perez, J.; Sanchez-Soto, M.; Velasco, J.; Santana, O.; Maspoch, M.L. The Essential Work of Fracture (EWF) method—Analyzing the Post-Yielding Fracture Mechanics of polymers. *Eng. Fail. Anal.* **2009**, *16*, 2604–2617. [CrossRef]

22. Pegoretti, A.; Castellani, L.; Franchini, L.; Mariani, P.; Penati, A. On the essential work of fracture of linear low-density-polyethylene. I. Precision of the testing method. *Eng. Fract. Mech.* **2009**, *76*, 2788–2798. [CrossRef]

23. Pardoen, T.; Marchal, Y.; Delannay, F. Thickness dependence of cracking resistance in thin aluminium plates. *J. Mech. Phys. Solids* **1999**, *47*, 2093–2123. [CrossRef]

24. Pardoen, T. A method for determining the CTOD at cracking initiation-application to the characterization of the fracture toughness of copper. In Proceedings of the ECF13, San Sebastian 2000, San Sebastian, Spain, 6–9 September 2013.

25. Marchal, Y.; Walhin, J.-F.; Delannay, F. Statistical procedure for improving the precision of the measurement of the essential work of fracture of thin sheets. *Int. J. Fract.* **1997**, *87*, 189–199. [CrossRef]

26. Mouzakis, D.E.; Stricker, F.; Mulhaupt, R.; Karger-Kocsis, J. Fracture behaviour of polypropylene/glass bead elastomer composites by using the essential work-of-fracture method. *J. Mater. Sci.* **1998**, *33*, 2551–2562. [CrossRef]

27. Elmeguenni, M.; Naït-Abdelaziz, M.; Zaïri, F.; Gloaguen, J.M. Fracture characterization of high-density polyethylene pipe materials using the $$J$$ J-integral and the essential work of fracture. *Int. J. Fract.* **2013**, *183*, 119–133. [CrossRef]

28. Ching, E.C.Y.; Poon, W.K.Y.; Li, R.; Mai, Y.-W. Effect of strain rate on the fracture toughness of some ductile polymers using the essential work of fracture (EWF) approach. *Polym. Eng. Sci.* **2000**, *40*, 2558–2568. [CrossRef]

29. Tehran, A.C.; Heidari, F.; Chakherlou, T.N.; Najjar, R. Fracture toughness and fractographic investigation of polybutylene terephthalate/thermoplastic polyurethane binary blends reinforced by multi-walled carbon nanotubes using essential work of fracture approach. *J. Compos. Mater.* **2022**, *56*, 743–759. [CrossRef]

30. Karger-Kocsis, J.; Khumalo, V.; Bárány, T.; Meszaros, L.; Pegoretti, A. On the toughness of thermoplastic polymer nanocomposites as assessed by the essential work of fracture (EWF) approach. *Compos. Interfaces* **2013**, *20*, 395–404. [CrossRef]

31. Yang, J.-L.; Zhang, Z.; Zhang, H. The essential work of fracture of polyamide 66 filled with TiO_2 nanoparticles. *Compos. Sci. Technol.* **2005**, *65*, 2374–2379. [CrossRef]

32. Hassan, M.K.; Abdellah, M.Y.; ElAbiadi, T.S.; Mohamed, A.F.; Azam, S.; Marzouk, W. Essential Work of Fracture and Size Effect in Copper/Glass-Reinforced Epoxy Laminate Composites Used as MEMS Devices. *Am. J. Mech. Eng.* **2017**, *5*, 234–238. [CrossRef]

33. Abdellah, M.Y. Essential work of fracture assessment for thin aluminium strips using finite element analysis. *Eng. Fract. Mech.* **2017**, *179*, 190–202. [CrossRef]

34. Chandra, N. Evaluation of interfacial fracture toughness using cohesive zone model. *Compos. Part A Appl. Sci. Manuf.* **2002**, *33*, 1433–1447. [CrossRef]

35. Xia, Z.; Curtin, W.; Sheldon, B. A new method to evaluate the fracture toughness of thin films. *Acta Mater.* **2004**, *52*, 3507–3517. [CrossRef]

36. Lee, S.; Ji, W. Measurement of pure mode I fracture toughness at a sandwich interface and parametrization of the R-curve for a cohesive element. *Compos. Struct.* **2022**, *291*, 115599. [CrossRef]

37. Huang, Y.; Zolfaghari, N.; Bunger, A.P. Cohesive element simulations capture size and confining stress dependence of rock fracture toughness obtained from burst experiments. *J. Mech. Phys. Solids* **2022**, *160*, 104799. [CrossRef]

38. Lee, J.; Gao, Y.; Johanns, K.; Pharr, G. Cohesive interface simulations of indentation cracking as a fracture toughness measurement method for brittle materials. *Acta Mater.* **2012**, *60*, 5448–5467. [CrossRef]

39. Abdellah, M.Y. Delamination Modeling of Double Cantilever Beam of Unidirectional Composite Laminates. *J. Fail. Anal. Prev.* **2017**, *17*, 1011–1018. [CrossRef]

40. Shao, Y.; Duan, Q.; Qiu, S. Consistent element-free Galerkin method for three-dimensional crack propagation based on a phase-field model. *Comput. Mater. Sci.* **2020**, *179*, 109694. [CrossRef]

41. Kabir, H.; Aghdam, M.M. A generalized 2D Bézier-based solution for stress analysis of notched epoxy resin plates reinforced with graphene nanoplatelets. *Thin-Walled Struct.* **2021**, *169*, 108484. [CrossRef]

42. Mai, Y.-W.; Cotterell, B. On the essential work of ductile fracture in polymers. *Int. J. Fract.* **1986**, *32*, 105–125. [CrossRef]

43. Broberg, K. On stable crack growth. *J. Mech. Phys. Solids* **1975**, *23*, 215–237. [CrossRef]

44. Kuno, T. Deformation mechanism under essential work of fracture process in polycyclo-olefin materials. *Express Polym. Lett.* **2008**, *2*, 404–412. [CrossRef]

45. Wu, J.; Mai, Y.-W. The essential fracture work concept for toughness measurement of ductile polymers. *Polym. Eng. Sci.* **1996**, *36*, 2275–2288. [CrossRef]

46. Ward, I.M.; Hadley, D.W. *An Introduction to the Mechanical Properties of Solid Polymers*; John Wiley & Sons, Inc.: San Francisco, CA, USA, 1993.

47. Jones, R.M. *Mechanics of Composite Materials*; CRC Press: Boca Raton, FL, USA, 1998.

48. Mallick, P.K. *Composites Engineering Handbook*; CRC Press: Boca Raton, FL, USA, 1997.

49. Khashaba, U.A. In-plane shear properties of cross-ply composite laminates with different off-axis angles. *Compos. Struct.* **2004**, *65*, 167–177. [CrossRef]

50. Mohammed, Y.; Hassan, M.K.; El-Ainin, H.A.; Hashem, A. Effect of stacking sequence and geometric scaling on the brittleness number of glass fiber composite laminate with stress raiser. *Sci. Eng. Compos. Mater.* **2014**, *21*, 281–288. [CrossRef]

51. Khashaba, U.; Aldousari, S.; Najjar, I. Behavior of $[0]_8$ woven composites under combined bending and tension loading: Part I experimental and analytical. *J. Compos. Mater.* **2012**, *46*, 1345–1355. [CrossRef]

52.   Petrie, E.M. *Epoxy Adhesive Formulations*; McGraw Hill Professional: New York, NY, USA, 2005.
53.   *ASTM D3171*; Standard Test Methods for Constituent Content of Composite Materials. ASTM: West Conshohocken, PA, USA, 2011.
54.   Hagnestål, A.; Sellgren, U.; Andersson, K. Durable winch-based point absorbers. In Proceedings of the Ewtec 2017: The 12th European Wave and Tidal Energy Conference, Cork, Ireland, 27 August–1 September 2017.
55.   Shukla, M.J.; Kumar, D.S.; Mahato, K.K.; Rathore, D.; Prusty, R.K.; Ray, B.C. A comparative study of the mechanical performance of Glass and Glass/Carbon hybrid polymer composites at different temperature environments. *IOP Conf. Ser. Mater. Sci. Eng.* **2015**, *75*, 012002. [CrossRef]
56.   MInus, M.; Kumar, S. The processing, properties, and structure of carbon fibers. *JOM* **2005**, *57*, 52–58. [CrossRef]
57.   *ASTM D3039/D 3039M*; Standard Test Method for Tensile Properties of Polymer Matrix Composite Materials. ASTM: West Conshohocken, PA, USA, 1995.
58.   Available online: https://www.zwickroell.com/products/static-materials-testing-machines/universal-testing-machines-for-static-applications/materials-testing-machine-with-hydraulic-drive/ (accessed on 15 May 2022).
59.   Newman, J., Jr.; Haines, M.J. Verification of stress-intensity factors for various middle-crack tension test specimens. *Eng. Fract. Mech.* **2005**, *72*, 1113–1118. [CrossRef]
60.   Belytschko, T.; Black, T. Elastic crack growth in finite elements with minimal remeshing. *Int. J. Numer. Methods Eng.* **1999**, *45*, 601–620. [CrossRef]
61.   Melenk, J.; Babuška, I. The partition of unity finite element method: Basic theory and applications. *Comput. Methods Appl. Mech. Eng.* **1996**, *139*, 289–314. [CrossRef]
62.   Datta, D. Introduction to extended finite element (XFEM) method. *arXiv* **2013**, arXiv:1308.5208.
63.   Abdellah, M.Y.; Alsoufi, M.S.; Hassan, M.K.; Ghulman, H.A.; Mohamed, A.F. Extended Finite Element Numerical Analysis of Scale Effect in Notched Glass Fiber Reinforced Epoxy Composite. *Arch. Mech. Eng.* **2015**, *62*, 217–236. [CrossRef]
64.   Li, X.; Hallett, S.R.; Wisnom, M.R.; Zobeiry, N.; Vaziri, R.; Poursartip, A. Experimental study of damage propagation in Over-height Compact Tension tests. *Compos. Part A Appl. Sci. Manuf.* **2009**, *40*, 1891–1899. [CrossRef]
65.   Yang, D.; Karimi, H.; Aliha, M. Comparison of Testing Method Effects on Cracking Resistance of Asphalt Concrete Mixtures. *Appl. Sci.* **2021**, *11*, 5094. [CrossRef]
66.   Hahn, G.; Rosenfield, A. Local yielding and extension of a crack under plane stress. *Acta Met.* **1965**, *13*, 293–306. [CrossRef]
67.   Perez, N. Crack Tip Plasticity. In *Fracture Mechanics*; Springer: Dordrecht, The Netherlands, 2017; pp. 187–225.
68.   Abdellah, M.Y. Comparative study on prediction of fracture toughness of CFRP laminates from size effect law of open hole specimen using cohesive zone model. *Eng. Fract. Mech.* **2018**, *191*, 277–285. [CrossRef]
69.   Abdellah, M.Y.; Hassan, M.K.; Mohamed, A.F.; Backar, A.H. Cyclic Relaxation, Impact Properties and Fracture Toughness of Carbon and Glass Fiber Reinforced Composite Laminates. *Materials* **2021**, *14*, 7412. [CrossRef] [PubMed]
70.   Narasimhachary, S.; Saxena, A.; Newman, J. A double edge notch specimen design for tension–compression fatigue crack growth testing. *Eng. Fract. Mech.* **2012**, *92*, 126–136. [CrossRef]
71.   Yilmaz, S.; Yilmaz, T.; Kahraman, B. Essential work of fracture analysis of short glass fiber and/or calcite reinforced ABS/PA6 composites. *Polym. Eng. Sci.* **2014**, *54*, 540–550. [CrossRef]
72.   Yilmaz, S.; Yilmaz, T.; Arici, A.A. Effect of annealing process in water on the essential work of fracture response of ultra high molecular weight polyethylene. *J. Mater. Sci.* **2011**, *46*, 1758–1766. [CrossRef]
73.   Hashemi, S. Work of fracture of high impact polystyrene (HIPS) film under plane stress conditions. *J. Mater. Sci.* **2003**, *38*, 3055–3062. [CrossRef]
74.   Peres, F.M.; Tarpani, J.R.; Schön, C.G. An assessment of essential work of fracture testing method applied to medium density polyethylene (MDPE). *Eng. Fract. Mech.* **2013**, *105*, 136–151. [CrossRef]